Experimental Mechanics
DOI 10.1007/s11340-014-9889-8

Is There An Optimal Gauge Length for Dynamic Tensile Specimens?

Y. Rotbaum · D. Rittel

Received: 30 December 2013 / Accepted: 4 April 2014

Abstract This paper addresses the issue of the dynamic tensile specimen gauge length through an experimental-numerical approach. Emphasis is put on the combined issue of specimen equilibrium and uniformity of the stress and the strain fields in the gauge. The systematic comparison of long and short specimens reveals the unexpected, namely the superiority of the long specimen in terms of the strain and stress uniformity, which in turn affects the accuracy of the experimental stress–strain curve, while excellent force equilibrium is obtained. The feasibility of longer dynamic tensile specimens adds a new degree of freedom to the specimen's design, while allowing for characterization of materials at lower strain rates.

Keywords Dynamic tensile testing · Dynamic force equilibrium homogeneous stress/strain field · Specimen length · Low strain-rate

Introduction

Mechanical properties characterization is a critical stage of the materials' selection process which may affect structural design, hence reliability. This procedure must include the material response to compression and tension over a wide range of strain rates, since most materials tend to exhibit strain-rate dependency, a phenomenon which cannot be overlooked. The first step of the material characterization is the quasi-static regime, which deals with strain rates of the order of 10^{-4}–$1\left[\frac{1}{s}\right]$. The experimental methodology for that is well established and relatively easy to perform using, e.g., servo-hydraulic machines. The high strain rate experiments, in the range of 10^{-3}–$10^{4}\left[\frac{1}{s}\right]$ are usually carried out using the Kolsky apparatus, also known as the Split Hopkinson Pressure Bar (*SHPB*). The latter has been accepted for material characterization since its modern inception in 1949 [1]. The SHPB, originally designed for high strain rate compression testing of engineering materials, has been continuously modified over the years to accommodate tension [2], torsion [3, 4], and the combination of the above. The tension Kolsky apparatus was invented in the 1960's, and its principle is similar to that of the compression bar, except for a few minor changes involving the methodology for tensile wave initiation [5, 6]. Moreover, the specimen, which was simply inserted between the bars in compression, needs now to be attached to the tensile bars by means of threading for example. For Split Hopkinson Tensile bar (SHTB) testing, a basic requirement needs to be fulfilled just like for compression tests [7, 8], namely specimen dynamic equilibrium along with a uniform state of stress and strain. For brittle materials, the use of pulse shapers [9] has been shown to ensure specimen equilibrium. On the other hand, the usual prevailing assumption, based on the work of Hunter and Davies [10] is that after three waves roundtrips in the specimen, the latter experiences a state of equilibrium, namely $F_{in}=F_{out}$, where those stand for the applied forces on each side of the specimen. From a practical point of view, it is therefore commonly accepted that the *shorter* the specimen, the earlier equilibrium will be achieved. Such a situation is also deemed to ensure uniformity of the stress and strain fields, although recent work using digital image correlation [11, 12] or by F.E methods [13, 14] has challenged this assumption (Table 1).

Finally, one should note the existence of a "twilight zone" which covers the range of strain rates of the order of $10^{2}\left[\frac{1}{s}\right]$. Here, specialized machines, and/or complicated techniques [15] are needed to explore those "low" dynamic strain rates (high speed servo-hydraulic machines).

Y. Rotbaum · D. Rittel (✉)
Faculty of Mechanical Engineering, Technion, 32000 Haifa, Israel
e-mail: merittel@technion.ac.il

Published online: 03 May 2014

Table 1 Table of specimens and experimental conditions

Material	Number of Compression samples	Strain rate [1/s]	Number of Tension samples	Strain rate [1/s]
PH 15–5 condition A	10	620–1,800	14	70–600
Aluminum 7075 T6	10	600–2,000	13	80–700
4340 H+T	11	800–2,000	11	40–620

Note the relatively large sample size which is aimed at increasing statistical representatively of the results. All the results shown in the sequel are typical and were ascertained for each test separately

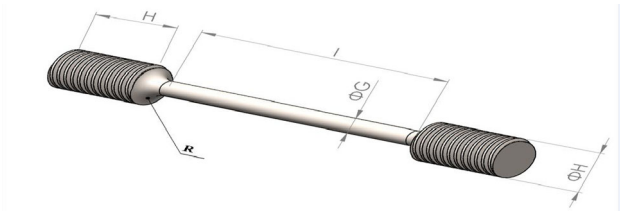

H [mm]	R [mm]	$\emptyset H$ [mm]	$\emptyset G$ [mm]	l [mm]
12	2.5	7.953	3	36 & 6

Fig. 1 Dynamic tensile specimen geometry and characteristic dimensions (mm)

This paper presents a hybrid experimental/numerical study which aims at re-assessing the validity of the above-mentioned assumptions and requirements, with emphasis on the lower part of the high strain rate testing range. Specifically, instead of making fundamental changes to existing SHTB systems, we investigate the feasibility of "long" specimens for dynamic tensile testing in light of the above-mentioned requirements, and compare the performance of such specimens to that of the conventional "short" ones. The paper will address the following three major issues of dynamic tensile testing:

1. The common belief that long specimens, in general, are not adequate for SHTB will be shown to be unfounded. Tests of "long" tensile specimens (36 mm gauge length) will reveal an excellent dynamic equilibrium.
2. Moreover, the "long" specimens will be shown, by means of numerical simulations, to exhibit a superior (homogeneous) stress and strain distribution than the shorter specimens.
3. Based on the previous two points just mentioned, it will be shown that one can easily perform material characterization in the (tensile) range of strain rates of $10^2-10^3\,\frac{1}{s}$

Experimental Setup

Materials and Specimens

Three materials were tested: 15–5 PH steel (condition A), 7075-T6 Aluminum alloy, and 4340 quenched and tempered steel (30HRB), all supplied as 12.7 mm diameter bars, and tested in the as-received condition. Tensile cylindrical specimens with end threads were machined from the bars. The specimens' dimensions are shown in Fig. 1. Two types of specimens were manufactured, namely long (36 mm gauge length), and short (6 mm gauge length), with gauge diameter of 3 mm. In addition, dynamic compression cylinders were machined from all the tested materials with a length and diameter of 6 mm. All the specimens were meant to examine the material behavior in both compression and tension, in the range of strain-rates of $10^2-10^3\left[\frac{1}{s}\right]$ except for the short tensile specimens that were meant for comparison with the behavior of the long specimens.

Dynamic Compression and Tension Setup

The dynamic compression specimens were tested in a standard 19.3 mm diameter Kolsky apparatus made of hardened C300 Maraging steel bars. The dynamic tensile specimens were tested in a 12.7 mm diameter Kolsky apparatus made of same material, which was loaded at the end of the incident bar with a 400 mm long tubular projectile. A momentum trap was brought initially in contact with the loaded flange of the incident bar, whose length was identical to that of the projectile bar, as shown in Fig. 2.

A Cordin 530 high-speed camera (HSC) was synchronized with the incident bar signals to capture the evolution of the specimens and neck inception, in order to separate the post-necking process from the uniform deformation phase.

Numerical Model

The dynamic tensile tests were modeled numerically using a finite element commercial package (Abaqus explicit F.E software [16]). The model was axisymmetric, and included the whole tensile experimental setup, except for the flange and the momentum trap. With the exception of the specimen fillet, the model was meshed with elements CAX4R, a 4-node bilinear axisymmetric quadrilateral, reduced integration, hourglass control element, with a typical seed size of $50\,\mu m$ along the specimen gauge, and $1{,}000\,\mu m$ along the Hopkinson bars. The elements size along the specimens gauge section was selected to be smaller than the convergence size (verified to be of the order of $900\,\mu m^2$ in preliminary calculations) in order to have an optimal resolution for small changes in the stress and strain fields, and improve detection of the onset of localization. The

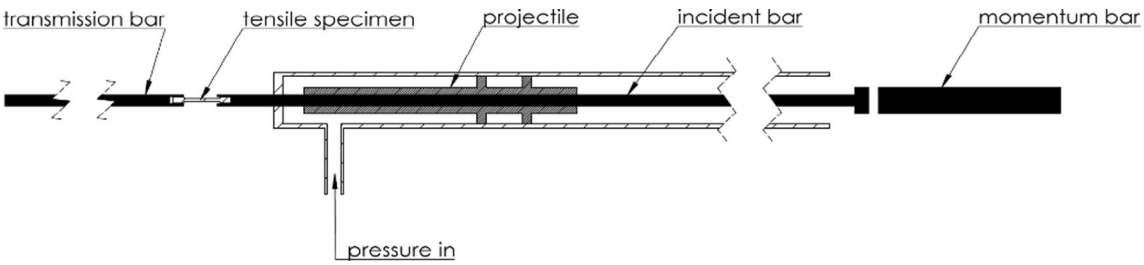

Fig. 2 Schematic representation of the Kolsky tension apparatus

boundary conditions of the simulation were taken from the experimental data as the amplitude of $\frac{v_{striker}}{2}$ applied to the free surface of the incident bar for the duration of the pulse. Specific elements were selected on the incident and the transmitted bars in order "replicate" the experimental strain gauges. Part of the meshed sample is shown in Fig. 3.

Results

Raw Signals

The dynamic tests, whether tensile or compressive, produce 3 signals that are recorded on the (bar) strain gauges, namely ε_i, ε_r, ε_t which stand for the incident, reflected and the transmitted pulses respectively. The signals were recorded with a Nicolet 440−12 bit differential oscilloscope.

Typical tension (a) and compression (b) signals are shown in Fig. 4, showing the quality and the level of separation of each signal.

Specimen Equilibrium

As already stated, a reliable stress–strain curve can be obtained only after verification of the dynamic specimen equilibrium. The forces applied on the specimen are given by:

$$F_{in} = E_b(\varepsilon_i + \varepsilon_t) \tag{1}$$

And

$$F_{out} = E_b(\varepsilon_t) \tag{2}$$

Where E_b is Young modulus of the bar, or in simpler from, if equilibrium is fulfilled

$$\varepsilon_i + \varepsilon_r = \varepsilon_t. \tag{3}$$

Figure 5 shows typical records of the applied forces for long (a) and short (b) tensile specimens, as well as for a compression specimen (c). Since the subject of dynamic compression has been extensively studied in the past, we will concentrate here on the tensile tests. Figure 5 shows an unexpected result, namely that the relatively long specimen exhibits a remarkable level of force equilibrium, which was only expected for the short specimen.

Once equilibrium is ascertained, the determination of the stress, strain and strain-rate is straightforward using the standard formulas:

$$v_{in} = C_b(\varepsilon_i - \varepsilon_t) \tag{4}$$

and

$$v_{out} = C_b(\varepsilon_t) \tag{5}$$

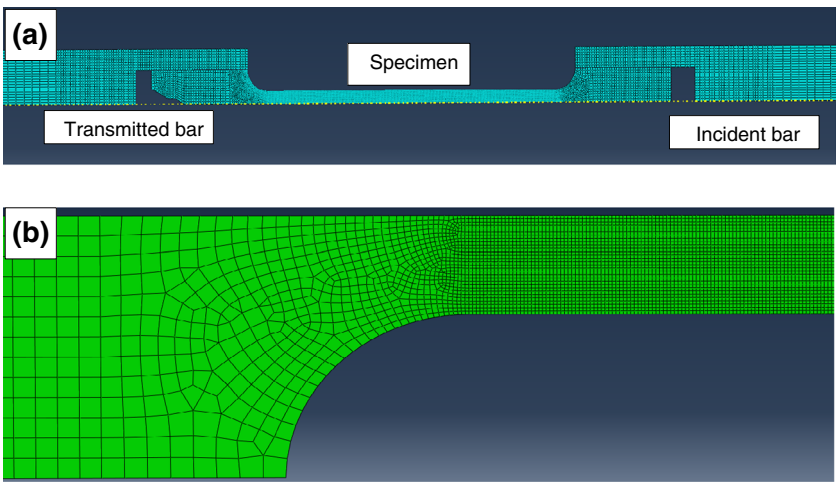

Fig. 3 (**a**) General meshing in the whole model. (**b**) Close-up on the specimen: shoulder, fillet and the gauge section

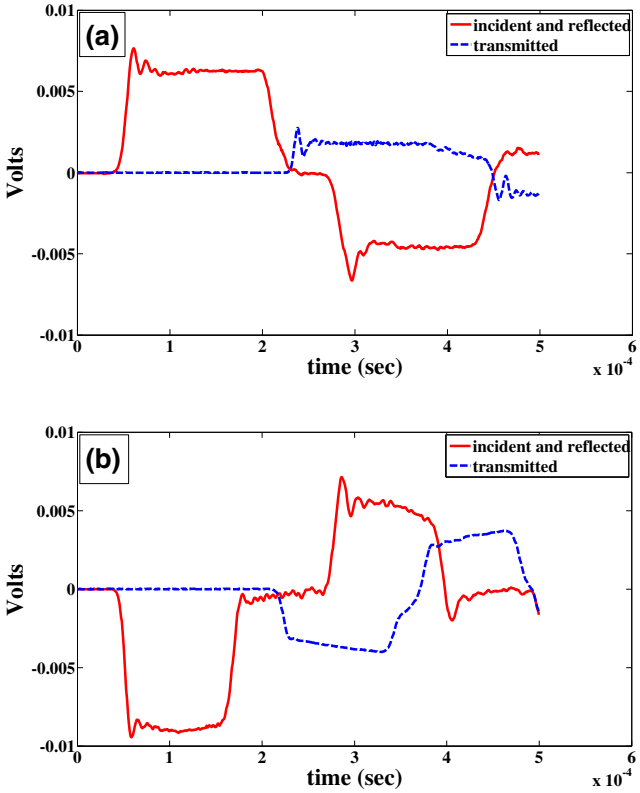

Fig. 4 (**a**) Raw signals from a-tensile experiment, (**b**) compression experiment

Where V_{in} and V_{out} are the interfacial specimen velocities and C_b is the bar wave speed. The nominal axial strain rate in the specimen is given by

$$\dot{\varepsilon}_S = \frac{v_{in} - v_{out}}{l_o} = \frac{C_b}{l_o}(\varepsilon_i - \varepsilon_r - \varepsilon_t) \tag{6}$$

consequently, the strain is given by:

$$\varepsilon_s = \int_0^t \dot{\varepsilon}(t)d\tau \tag{7}$$

And the stress is therefore:

$$\sigma_s = \frac{E_b A_b}{A_s}\varepsilon_t(t) \tag{8}$$

Note that, at this stage, one can only *assume* that the stress and strain are homogeneous, a point that deserves further verification as shown in the sequel. As stated before, the high speed photographic records were used to assess the exact time of the neck inception, so that beyond that point, both the stress and the strain cease to be homogeneous, if at all.

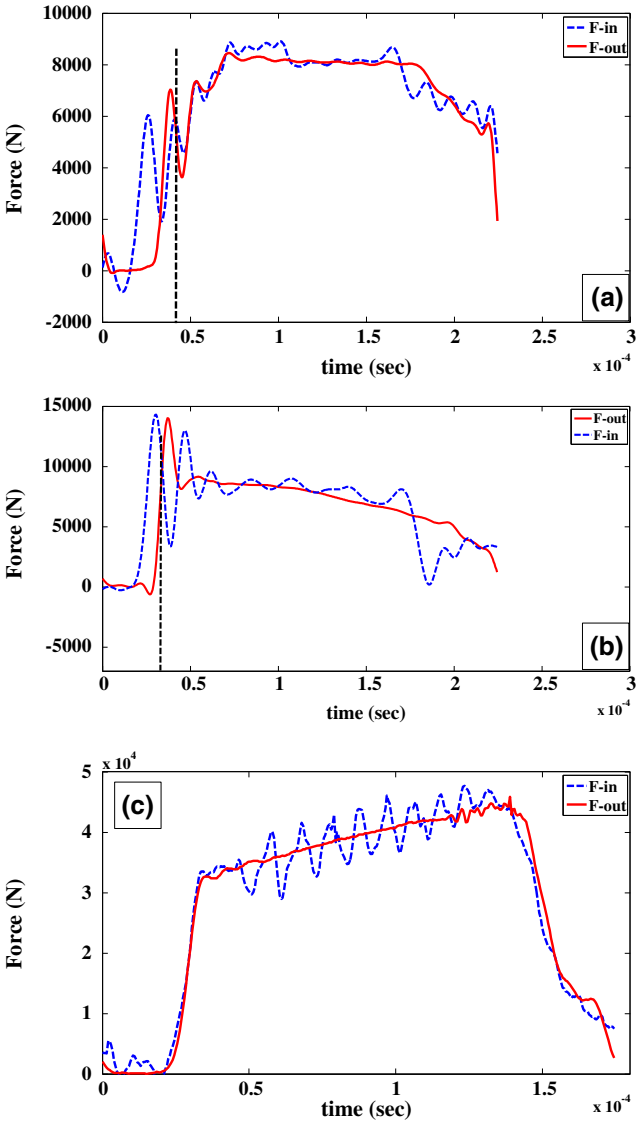

Fig. 5 (**a**) F_{in} and F_{out} showing equilibrium in the long tensile specimen. The small spike in the F_{out} initial signal results from data processing artifacts and has no physical meaning. (**b**) Same for the short tensile specimen. (**c**) Same for a compression experiment

Once the experiments are carried out, the numerical model must be verified and validated. The simulation provides the possibility to carefully examine the stress and strain distribution throughout the experiment, as discussed next.

Numerical Results

Model Verification

The first step of the simulation was to compare the recorded raw experimental signals to the calculated ones. A typical example of the numerical reproduction of the raw experimental signals is shown in Fig. 6. As can be seen in that figure, the

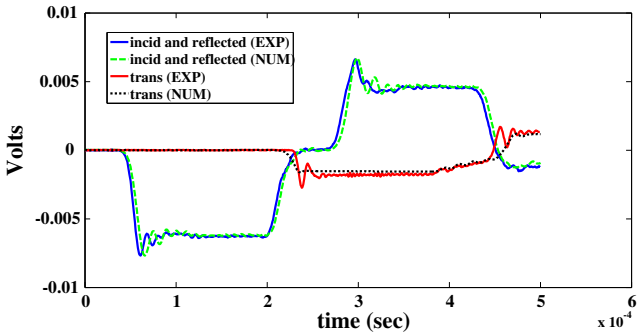

Fig. 6 Comparison between experimental and calculated raw signals

agreement between the numerical and the experimental raw signals is excellent.

Specimen equilibrium

The next step was the numerical verification of the specimen equilibrium. For this purpose, a long and a short specimen were subjected to the very same input velocity profile, with the difference that the amplitude (velocity) of each profile was scaled to the specimen gauge length in order to reproduce a similar nominal strain rate. As shown in Fig. 7, the numerical simulations indicate an excellent state of equilibrium for *both* the long (a) and short (b) specimens, in full accord with the previous experimental determination (Fig. 5 (a) and (b)). Note that the long specimen reaches equilibrium after approximately 40–50 μsec, while the short specimen does it after approximately 30–35 μsec. Those values are shown as dashed lines in Fig. 7a, similar to Fig. 5.

From here on, one can proceed to investigate the homogeneity of the stress and the strain fields in the tensile specimens, based on the numerical simulations.

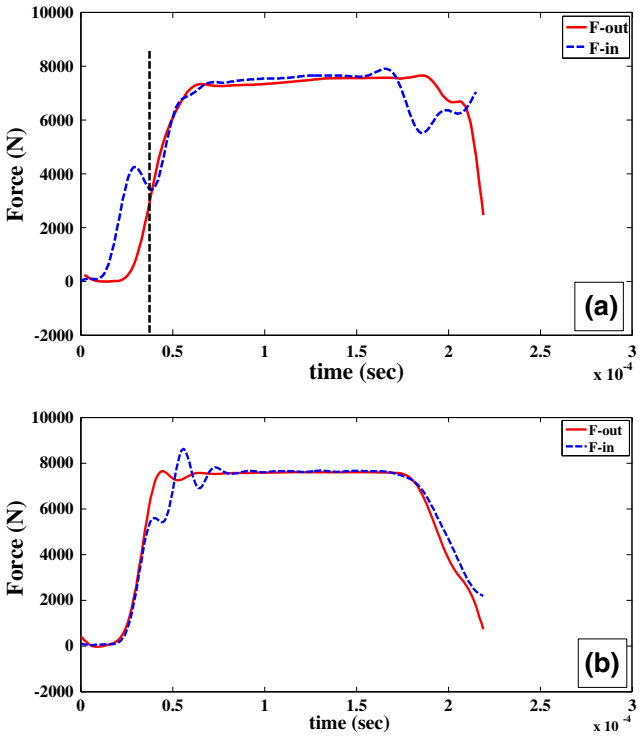

Fig. 7 (**a**) F_{in} and F_{out} as a measure of equilibrium in tensile numerical experiment with long specimen. The small spike in the initial signal results from data processing artefacts and has no physical meaning". (**b**) F_{in} and F_{out} as a measure of equilibrium in tensile numerical experiment with short specimen. The vertical dashed line indicates the initial region of non-equilibrium and the state of equilibrium thereafter

Stress and strain fields

Two main time sequences were defined according to the experimental behavior, namely before and after equilibrium (0–40 μsec and 40–180 μsec respectively). Figs. 8 and 9 shows the calculated evolution of the *longitudinal* stress distribution in the short and long specimens. Each figure is split into two phases, namely (a) before and (b) after equilibrium, according to the times needed to reach equilibrium. For each figure, the specimen's length is normalized to a maximum value of 1.

The stress recorded in the simulations of the short specimen (Fig. 8) looks relatively homogeneous before and after equilibrium. With that, one can also observe that the actual gauge normalized length over which the stress is homogeneous is of the order of 0.7, indicating that the effective gauge length is shorter than the nominal, or simply that end effects are noticeable.

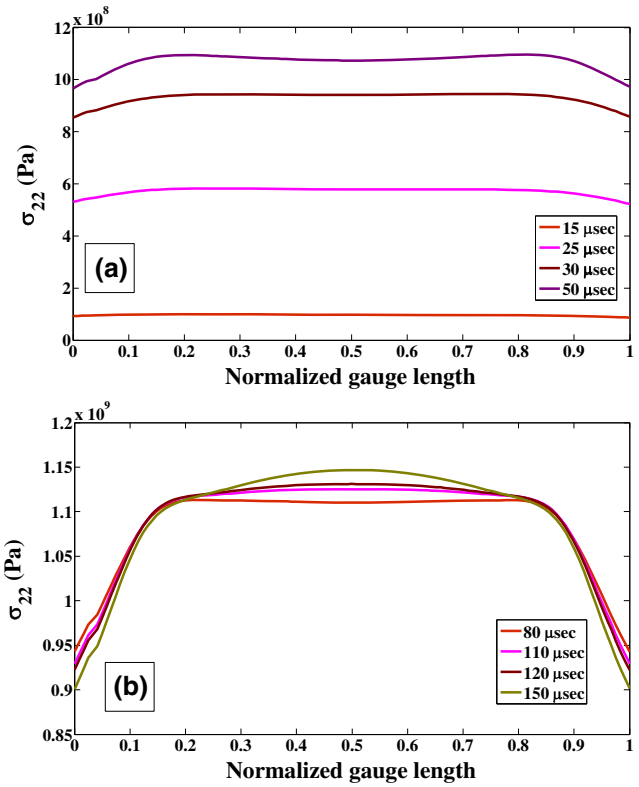

Fig. 8 (**a**) Longitudinal stress distribution in (a) the short specimen before equilibrium, (**b**) the short specimen after equilibrium

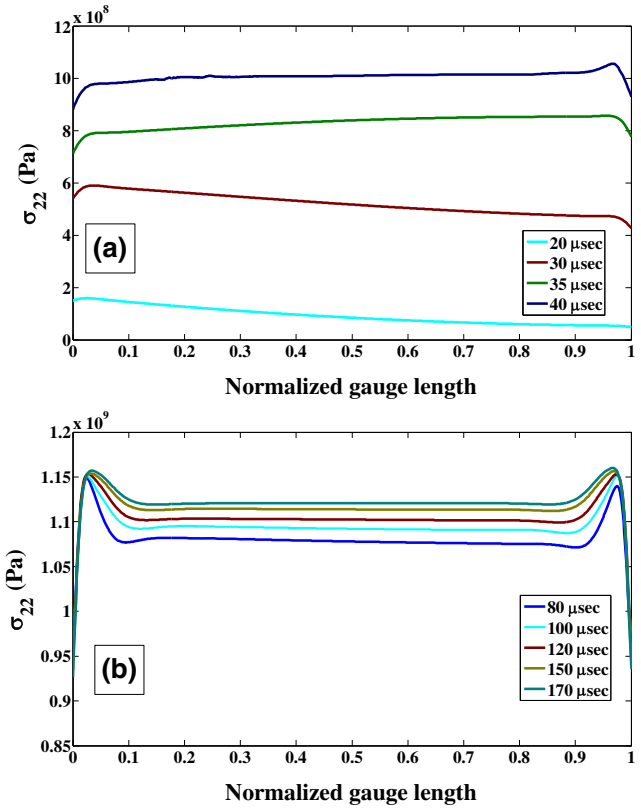

Fig. 9 (**a**) Longitudinal stress distribution in (a) the long specimen before equilibrium, (**b**) the long specimen after equilibrium

The long specimens (Fig. 9) exhibit a generally uniform stress distribution. The initial lack of homogeneity during the non-equilibrium phase vanishes rapidly. However, just like in the previous case, one can notice that end effects still prevail over about 0.2 of the normalized gauge length, thereby reducing it to 0.8. Moreover, while the short specimen experiences a steep stress gradient close to its end-pieces, the long specimen just experiences a small localized stress peak. Altogether, those results show that the stress distribution at equilibrium is not totally homogeneous, irrespective of the gauge length. However, the same results show that even for a long specimen, the stress is overall reasonably homogeneous.

The distribution of the Mises stress along the gauge section of the short (a) and long (b) specimens is presented in Fig. 10.

Similar conclusions can be deriving from the behavior of the Mises stress while comparing it to the longitudinal stress in the short specimens. In the long specimens on the other hand, there is a significant improvement in the distribution recorded as Mises stress. The lack of inhomogeneity in both edges of the gauge section is now much less marked.

Let us consider now the evolution of the *equivalent plastic strain* for those specimens, as shown in Figs. 11 and 12, with the same distinction of pre (a) and post (b) equilibrium. Figure 11 shows that the equivalent plastic strain of the short specimen is not uniform (parabolic) during both phases, to be contrasted with the previous relative uniformity of the stress distribution.

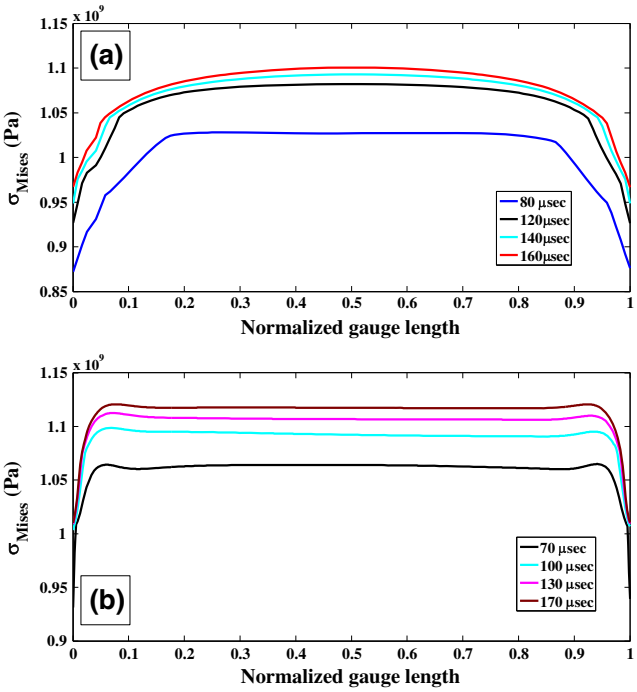

Fig. 10 Mises stress distribution in (**a**) the short and (**b**) long specimens after equilibrium

By contrast, the long specimens (Fig. 12) reveal a high degree of uniformity, mostly once equilibrium is established. The results are similar to those of the Mises stress as can be seen. In other words, the long specimen exhibits *both* stress and strain uniformity, a result that was rather unexpected.

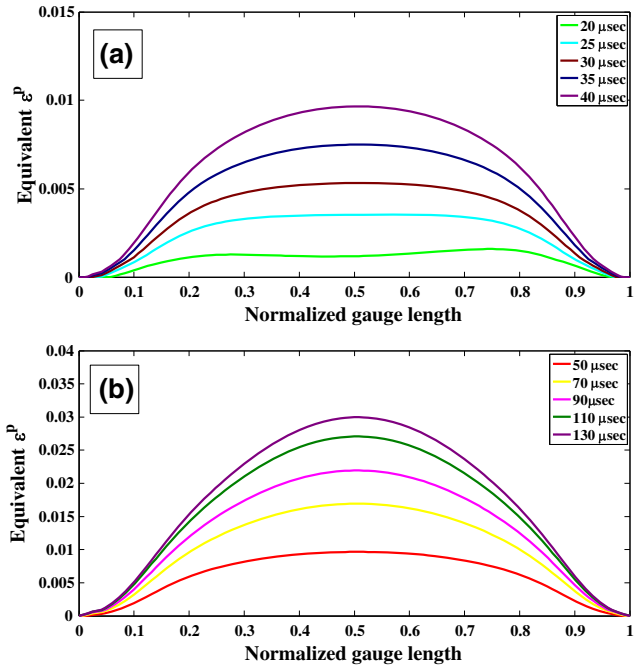

Fig. 11 Equivalent plastic strain distribution in the short specimen (**a**) before, and (**b**) after equilibrium

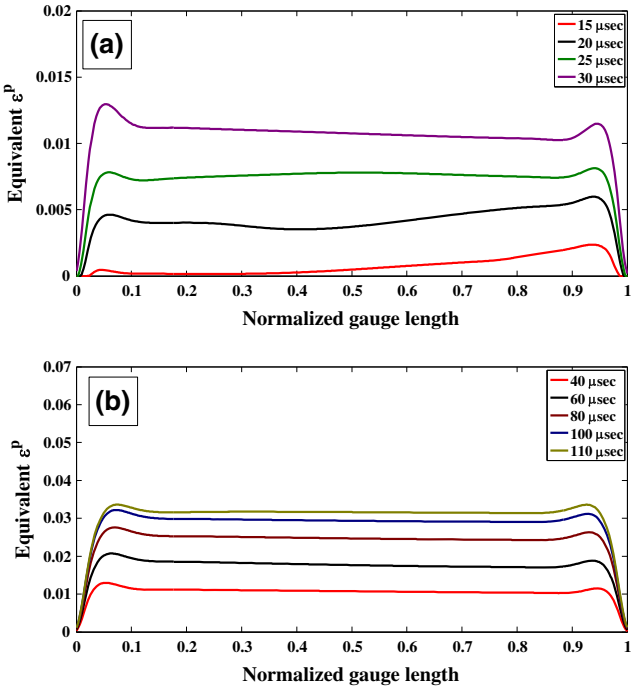

Fig. 12 Equivalent plastic strain distribution in the long specimen, (**a**) before, and (**b**) after equilibrium

Another point that deserves attention is the deformation in the fillets region, as addressed using digital image correlation [17]. Examination of the displacement in the simulations, whether measured from the gauge section only or from the fixed-ends displacements reveals that in the present case, the fillets' area does not participate in the overall deformation process to any significant extent. Moreover, the calculated equivalent plastic strain in the whole sample (Fig. 13) shows a minor deformation in this region.

To summarize the main results of the numerical simulations, it appears that force equilibrium, while being a necessary condition for a valid stress–strain determination, is apparently not a sufficient condition. Numerical simulations must be used to ascertain the degree of stress and strain homogeneity in the gauge section. Another important point is noted, namely that the use of a longer specimen ensures a more uniform distribution of both the stress and the plastic strain along the gauge length, contrary to the conventional wisdom mentioned in the introduction.

Experimental Results

As a foreword, it should be noted that the stress–strain curves shown in the sequel are not the main point of the paper, but are in fact determined once all other considerations, such as equilibrium, are sorted out. Since rather long specimens were used and validated in this study, very low strain rates were reachable, with satisfactory force equilibrium. In other words, the option of a variable specimen length provides a new degree of freedom in the experimental design.

Stress Strain Curves

Three different materials were successfully tested, which implies that equilibrium conditions are not material-dependent, a point that was expected. As an example, typical tensile stress strain curves are shown in Fig. 14 for annealed15-5 PH steel.

The strain achieved in the experiments is relatively low due to the original design of the tensile apparatus used in this article, in which the projectile length is limited (400 [mm]). However, this does not detract from the validity of the experiments. In addition, the typical behavior for compression of this material is shown in Fig. 15.

The compressive strain rates were in the upper range of $10^2\left[\frac{1}{s}\right]$, thus complementing the tensile range of strain-rates.

From Figs. 14 and 15 one can note that, whereas the flow stress is comparable between tension and compression, the strain hardening is quite different. The compressed material exhibits some strain-hardening which vanishes in tension. This difference, reported for the 15–5 PH steel, was also observed for 7075-T6 aluminum alloy (not shown here). We did not investigate the exact reasons for this lack of symmetry, which is not at all uncommon, as it has been identified earlier as a "strength differential effect (see e.g. Spitzig et al. [18]) in high strength steels, as will as in many magnesium alloys. It can be surmised here is that the materials investigated here are

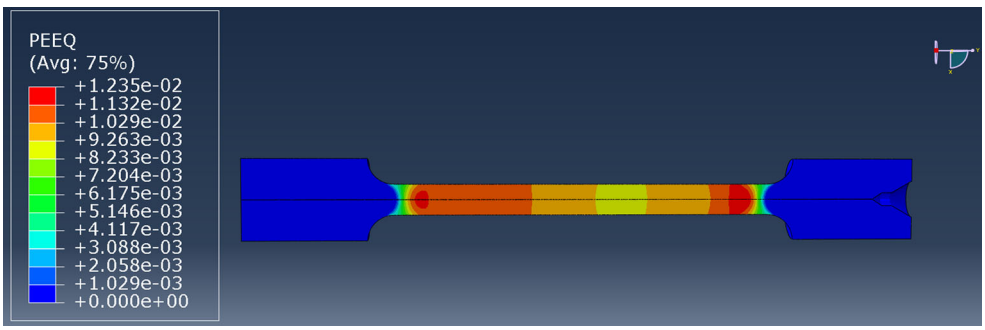

Fig. 13 Numerical snapshot showing the equivalent plastic strain of a 36 [mm] gauge length tensile specimen submitted to a tensile strain rate of $200\left[\frac{1}{s}\right]$, 80[µsec] after the wave front hits the sample. Note that the fillets do not deform to any significant extent

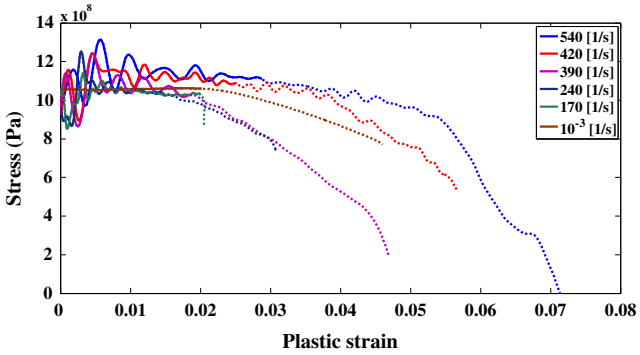

Fig. 14 Tensile stress-plastic strain curves from the experiments on annealed15-5 PH steel. *Dashed lines* are post-necking. (Therefore not strictly valid)

apparently pressure sensitive to some extent, but a detailed investigation of this issue is beyond the scope of the present paper. Yet, this observation emphasizes again the relevance of dynamic testing in *both* tension and compression. Moreover, since low tensile strain-rates are easily achievable with long specimens, the combined tension and compression tests can be used to characterize a material in a seamless manner over a wide range of strain-rates, therefore bridging the traditional gap that exists around the $10^2\left[\frac{1}{s}\right]$.

Discussion

Starting from a quest for dynamic tensile experiments in the low strain rate regime $\left(10^2\left[\frac{1}{s}\right]\right)$, by using relatively long specimens (36 [mm] vs. 6 [mm]), turned out eventually into a thorough reassessment of well-established beliefs that the shorter the specimen, the better the force equilibrium, implying automatically a uniform stress/strain distribution along the specimens' gauge length.

Systematic testing of over forty specimens made of 3 different alloys revealed the fact that long specimens can rapidly achieve an excellent state of force equilibrium, contrary to the common belief. Finite element simulations of short and long specimens at comparable strain rates show that force equilibrium alone does not warrant uniformity of the stress and strain in the specimen. While both the short and the long specimens achieve rapidly a state of force equilibrium, the stress and strain fields are significantly more homogeneous in the longer specimens, where the plastic strain is the most sensitive issue. Stated otherwise, the equivalent plastic strain is far from being homogeneous in the short specimens. As a result, the reliability of the experimental stress–strain curves obtained with such specimens may be questionable, while this is not the case for the longer ones.

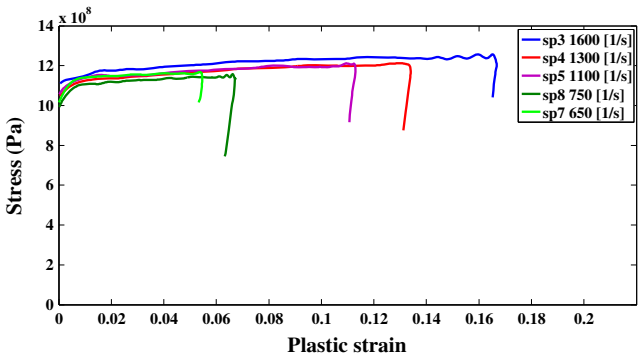

Fig. 15 Compression stress-plastic strain curves from the experiments on annealed15-5 PH steel

Another outcome of this work is the ability to reach the low end of dynamic tensile strain rates using those longer specimens, which, if the material is symmetrical in tension and compression, bridges the gap between the quasi-static strain rates and the higher range traditionally investigated using the Kolsky apparatus.

However, if high strain rates are desirable, the latter can be achieved without compromising equilibrium and uniformity issues, using an intermediate gauge length specimens', e.g. 12 [mm] long, as shown in the Appendix, showing strain rates of the order of 2,000 $\left[\frac{1}{s}\right]$.

Another interesting outcome of this study lies in the different strain buildup in the specimen's gauge length. Considering the short specimen, one notes the parabolic nature of the strain distribution which reaches a peak at mid-length of the specimen. As a result, necking and subsequent failure are expected to develop in this location. However, for the longer specimens, the strain distribution is homogeneous along the gauge length. This state of homogeneity allows for the subsequent development of the neck and failure at any location along the gauge length without preference for its mid-length, as reported experimentally in [19] and [20].

Conclusions

- Long gauge length specimens (e.g. 36 [mm]) are preferable for obtaining a reliable dynamic tensile stress–strain curve.
- In those specimens, force equilibrium corresponds to a uniform stress and strain distribution in the long specimens.
- Force equilibrium does not mean a uniform stress/strain state for the short (6 [mm]) specimens, which in turns affects the reliability of the determined mechanical characteristics of the investigated material.
- The use of longer specimens allows for dynamic testing in the low $\left(100\left[\frac{1}{s}\right]\right)$ strain rate regime.
- When higher strain rates are required, e.g. $\left(2000\left[\frac{1}{s}\right]\right)$, the selection of 12 (mm) long specimens will ensure both force equilibrium and a uniform state of stress and strain.
- While short specimens are expected to fail at mind-length as a result of their parabolic strain distribution, the longer

specimens can fail anywhere along the gauge length due to the uniformity of the strain field, as observed in previous experimental work [20].

Appendix

The long gauge length specimens have already been shown numerically and experimentally to be feasible for dynamic tensile testing in the low strain rate regime, while satisfying dynamic force equilibrium with homogeneous stress and strain along the gauge length. If higher strain rate are considered, of the order of $\left(2000\left[\frac{1}{s}\right]\right)$ for example, it is possible to reduce the length of the gauge length, without compromising any of the basic requirements for valid testing. Sample with 12 [mm] gauge length were tested and modeled in order to validate the uniformity of the stress and the strain in the gauge length during the experiment in the pre-necking phase. The Mises (a) and the longitudinal (b) stress, together with the equivalent plastic strain (c) distribution are all shown in Fig. 16.

From this figure, one can observe that all the parameters remain uniform as they were in the long specimen. The ability the decrease the gauge length and still fulfill the basic requirements of the Hopkinson experiments, emphasize the role of numerical simulations when designing the optimal specimen geometry for dynamic tensile experiments.

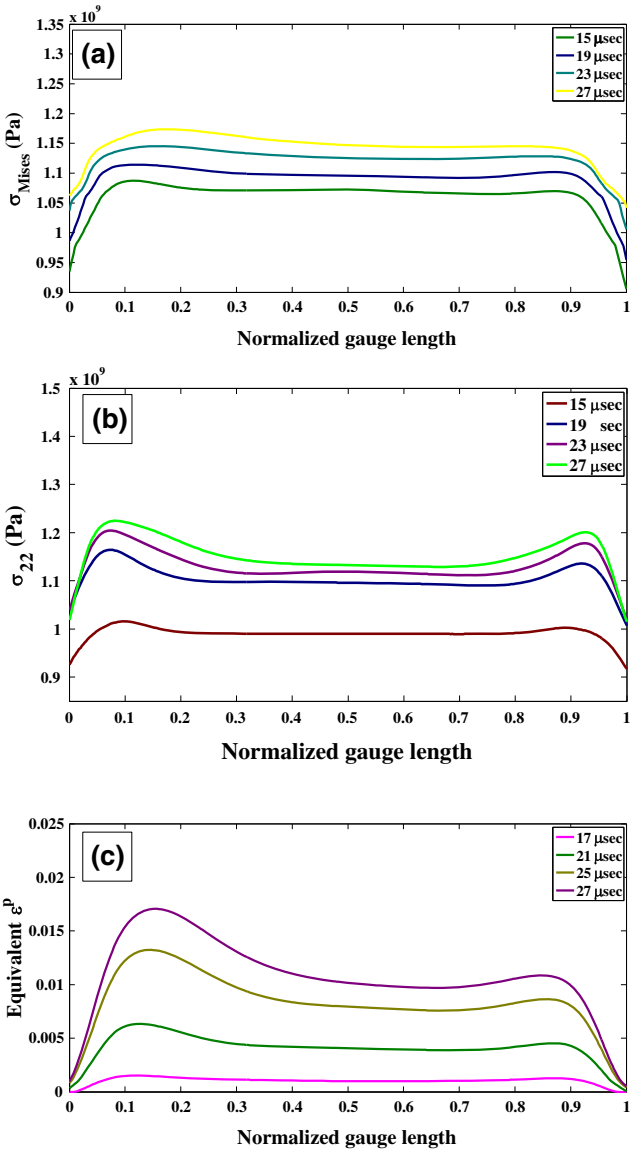

Fig. 16 (**a**) (**b**) (**c**) the distribution in 12 [mm] gauge section specimens in the pre-necking stage of the Mises stress the longitudinal stress and the equivalent plastic strain respectively

References

1. Kolsky H (1949) An investigation of the mechanical properties of materials at very high rates of loading. vol. 62: IOP Publishing, p.676
2. Harding J, Wood EO, Campbell JD (1960) Tensile testing of materials at impact rates of strain. vol. 2: SAGE Publications, p.88
3. Lewis J, Campbell J (1972) The development and use of a torsional Hopkinson-bar apparatus. Exp Mech 12:520
4. Baker WEYCHUoTEMRL. Strain-rate effects in propagation of torsional plastic waves. Austin, Tex.: Engineering Mechanics Research Laboratory, University of Texas, 1965
5. Ellwood S, Griffiths L, Parry D (1982) A tensile technique for materials testing at high strain rates. J Phys E: Sci Instrum 15:1169
6. Gerlach R, Kettenbeil C, Petrinic N (2012) A new split Hopkinson tensile bar design. Int J Impact Eng
7. Mohr D, Gary G, Lundberg B (2010) Evaluation of stress–strain curve estimates in dynamic experiments. Int J Impact Eng 37:161
8. Subhash G, Ravichandran G (2000) Mechanical Testing and Evaluation. ASM Int 8:497
9. Frew D, Forrestal MJ, Chen W (2002) Pulse shaping techniques for testing brittle materials with a split Hopkinson pressure bar. Exp Mech 42:93
10. Davies E, Hunter S (1963) The dynamic compression testing of solids by the method of the split Hopkinson pressure bar. J Mech Phys Solids 11:155
11. Gilat A, Schmidt T, Tyson J (2006) Full field strain measurement during a tensile split Hopkinson bar experiment. J Phys IV (Proceedings) 134:687, EDP sciences
12. Song B, Antoun BR, Jin H (2010) Dynamic Tensile Characterization of a 4330-V Steel with Kolsky Bar Techniques. Exp. Mech. 1
13. Rodriguez J, Sanchez-Galvez V, Navarro C (1994) Numerical assessment of the dynamic tension test using the split Hopkinson bar. J. Test. Eval.;(United States) 22
14. Klepaczko J (2005) Review on critical impact velocities in tension and shear. Int J Impact Eng 32:188
15. Othman R, Gary G (2007) Testing aluminum alloy from quasi-static to dynamic strain-rates with a modified Split Hopkinson Bar method. Exp Mech 47:295
16. Hibbett, Karlsson, Sorensen, Hibbitt (1998) ABAQUS/standard: User's Manual. Vol. 1. Karlsson & Sorensen, Hibbitt

17. Gilat A, Schmidt T, Walker A (2009) Full field strain measurement in compression and tensile split Hopkinson bar experiments. Exp Mech 49:291
18. Spitzig WA, Sober RJ, Richmond O (1976) The effect of hydrostatic pressure on the deformation behavior of maraging and HY-80 steels and its implications for plasticity theory. Metall Trans A 7:1703
19. Osovski S, Rittel D, Rodríguez-Martínez JA, Zaera R (2013) Dynamic tensile necking: influence of specimen geometry and boundary conditions. Mechanics of Materials
20. Rittel D, Rotbaum Y, Rodriguez-Martinez J, Sory D, Zaera R (2014) Dynamic necking of notched tensile bars: an experimental study. Exp Mech. doi:10.1007/s11340-014-9860-8